

Cite this: *Phys. Chem. Chem. Phys.*, 2012, **14**, 5132–5138

www.rsc.org/pccp

PAPER

# Sonochemical formation of iron oxide nanoparticles in ionic liquids for magnetic liquid marble<sup>†</sup>

Shiguo Zhang, Yan Zhang, Ying Wang, Shimin Liu and Youquan Deng\*

Received 22nd November 2011, Accepted 9th February 2012

DOI: 10.1039/c2cp23675c

Ionic liquids (ILs)-stabilized iron oxide ( $\text{Fe}_2\text{O}_3$ ) nanoparticles were synthesized by the ultrasonic decomposition of iron carbonyl precursors in  $[\text{EMIm}][\text{BF}_4]$  without any stabilizing or capping agents. The  $\text{Fe}_2\text{O}_3$  nanoparticles were isolated and characterized by X-ray powder diffraction, transmission electron microscopy and susceptibility measurements. The physicochemical properties of ILs containing magnetic  $\text{Fe}_2\text{O}_3$  nanoparticles (denoted as  $\text{Fe}_2\text{O}_3@[\text{EMIm}][\text{BF}_4]$ ), including surface properties, density, viscosity and stability, were investigated in detail and compared with that of  $[\text{EMIm}][\text{BF}_4]$ . The  $\text{Fe}_2\text{O}_3@[\text{EMIm}][\text{BF}_4]$  can be directly used as magnetic ionic liquid marble by coating with hydrophobic and unreactive polytetrafluoroethylene (PTFE), for which the effective surface tension was determined by the puddle height method. The resulting magnetic ionic liquid marble can be transported under external magnetic actuation, without detachment of magnetic particles from the marble surface that is usually observed in water marble.

## 1. Introduction

Ionic liquids (ILs) possess unique physicochemical properties including negligible vapor pressure, wide liquid temperature range, intrinsic ionic conductivity, supramolecular network, low toxicity, and acceptable electrochemical stability, *etc.*,<sup>1–3</sup> which have been used for synthesis of functional nanostructured materials such as iron<sup>4,5</sup> or iron oxide<sup>6–10</sup> nanoparticles. For instance, the synthesis of iron or iron oxide nanoparticles by the thermal or photolytic decomposition of iron carbonyl with stabilizers in imidazolium ILs was recently reported.<sup>5,6,8,9</sup> A small amount of IL  $[\text{BMIm}][\text{BF}_4]$  was found to be an efficient aid for microwave heating of nonpolar dibenzyl ether in high temperature solution-phase synthesis of monodisperse magnetite  $\text{Fe}_3\text{O}_4$  nanoparticles.<sup>10</sup>  $\alpha\text{-Fe}_2\text{O}_3$  with various morphologies has been successfully synthesized *via* an IL-assisted hydrothermal synthetic method.<sup>7</sup> However, these methods often need rigorous conditions such as high temperature ( $>250\text{ }^\circ\text{C}$ ), or additional stabilizing agents and cosolvents. More recently, the autocatalytic sonolysis of  $\text{Fe}(\text{CO})_5$  in IL  $[\text{BMIm}][\text{Tf}_2\text{N}]$  in argon flow was reported to provide non-aggregated uniform Fe nanoparticles with a mean size of 3 nm,<sup>4</sup> for which no additional ligands or stabilizing agents are needed, since ILs can provide electrostatic protection in the form of a protective shell for nanoparticles.

However, to the best of our knowledge, iron oxide nanoparticles have never been obtained in ILs by using sonochemical synthesis.

On the other hand, liquid marbles, which are stabilized by adsorbed hydrophobic particles at gas–liquid interfaces, have attracted increasing attention<sup>11–19</sup> in view of their potential applications in revealing water pollution, micro- and ferrofluidic devices,<sup>17,20</sup> micro-reactors,<sup>21,22</sup> gas sensing,<sup>23,24</sup> micro-pumps,<sup>25</sup> cosmetics, *etc.* Stimulus responsive liquid marbles have been reported recently.<sup>18,26</sup> Because of the absence of a contact line, liquid marbles are in a non-wetting situation on any surface and thus behaves as a micro-reservoir able to move quickly without any leakage. Since magnetic actuation has advantages in large and long-range forces and very low interaction with nonmagnetic media, liquid marbles that can be easily magnetically actuated have been prepared by co-application of hydrophobic lycopodium particles and iron microparticles on aqueous drops<sup>15</sup> or by dispersing iron microparticles or  $\text{Fe}_2\text{O}_3$  nanoparticles into the aqueous drops.<sup>14,15,19</sup> However, most liquid marbles reported so far have been based on aqueous liquid, which inevitably causes the problem of evaporation and collapse under ambient conditions because of the coated permeable shell of the liquid marbles. To obtain stable liquid marbles, many approaches, including doping water with glycerol, modification of the hydrophobic particles, or immersing the liquid marbles in organic liquids, have been used to depress the evaporation rate.<sup>16,27</sup> However, the insolubility of organic reagents in water and glycerol limited their applications. Moreover, in the magnetic aqueous marble system, there is a problem including either the detachment of magnetic particles from the marble

Center for Green Chemistry and Catalysis, Lanzhou Institute of Chemical Physics, Chinese Academy of Sciences, Lanzhou, 730000, China. E-mail: ydeng@licp.cas.cn; Fax: +86 09314968141; Tel: +86 09314968141

<sup>†</sup> Electronic supplementary information (ESI) available. See DOI: 10.1039/c2cp23675c

surface (phase separation) due to the action of magnetic force, leading to the loss of magnetic response, or the aggregation of the magnetic particles under the magnetic field, resulting in uneven pulling and deformation of the droplet.<sup>15</sup>

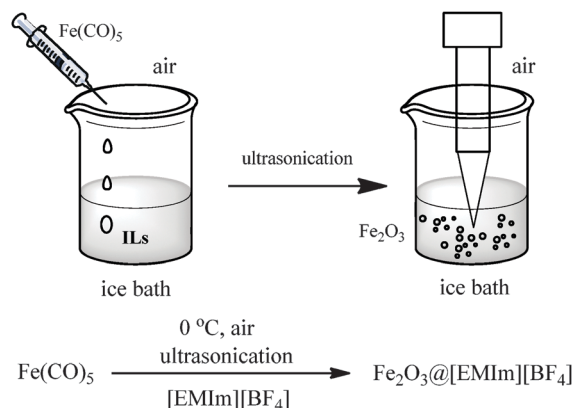
Ionic liquid marble, as initially reported by Gao and McCarthy,<sup>28</sup> will not only help to avoid evaporation and thus can be used under some extreme conditions either at temperatures above 373 K or below 273 K, or under high vacuum conditions, but also expand the application area of liquid marble due to the highly selective solubility of ILs in organic or inorganic solutes. Moreover, ILs have recently attracted much attention in microfluidics such as electrowetting and microreactors, and the controlled manipulation of minute quantities of ILs on a surface becomes a challenging problem due to the high viscosity and less surface tension (caused less contact angle to form a droplet) of ILs. The magnetic ionic liquid marble could be a promising candidate to solve this problem. Although many types of magnetic fluid that are stable dispersions of magnetic nanoparticles in ILs were recently reported,<sup>29–32</sup> the ILs-based magnetic ionic liquid marble, however, is not studied.

In this work, we report on one-step facile synthesis of iron oxide nanoparticles in IL in air by ultrasonic decomposition of  $\text{Fe}(\text{CO})_5$  in the absence of any other stabilizing surfactants and capping agents (Scheme 1). The resulted stable iron oxide nanoparticles/IL system can be directly used to prepare the millimetre-sized magnetic ionic liquid marble, which combined the intrinsic nature of ILs and magnetic properties, and can be easily transported with applied magnetic field. Moreover, accumulation of magnetic particles that inevitably confronted in general water marbles was absent in this magnetic ionic liquid marble.

## 2. Experiment

### Chemicals

PTFE powder was from Alfa Aesar.  $\text{Fe}(\text{CO})_5$  was supplied as a gift by Prof. Bin Hu in Lanzhou Institute of Chemical Physics, Chinese Academy of Sciences. 1-Ethyl-3-methylimidazolium tetrafluoroborate ([EMIm][BF<sub>4</sub>]) was synthesized by a two-step procedure and confirmed by the <sup>1</sup>H and <sup>13</sup>C NMR spectra ( $\delta_{\text{H}}$  (acetone-*d*<sub>6</sub>) = 1.532–1.569 (t, 3H),



**Scheme 1** Synthesis of iron oxide nanoparticles in [EMIm][BF<sub>4</sub>].

4.028 (s, 3H), 4.3352–4.407 (t, 2H), 7.686 (s, 1H), 7.760 (s, 1H), 8.9975 (s, 1H);  $\delta_{\text{C}}$  (acetone-*d*<sub>6</sub>) = 15.542, 36.414, 45.570, 122.962, 124.635, 137.269). [EMIm][BF<sub>4</sub>] was dried under reduced pressure at 80 °C for 4 h prior to ultrasonication.

### Synthesis of $\gamma\text{-Fe}_2\text{O}_3$ /[EMIm][BF<sub>4</sub>]

To 20 ml of [EMIm][BF<sub>4</sub>] placed in a 50 ml round-bottomed flask in an ice bath was added 0.5 ml of iron pentacarbonyl ( $\text{Fe}(\text{CO})_5$ ) by a syringe. The ultrasound probe was adjusted to below the liquid surface about 1 cm, and then the mixture was ultrasonicated at 100 mW power (JY92-II, Scientz Biotechnology Co., Ltd) for 1.5 h.

### Instrumentation and characterization

The viscosity was measured on a Brookfield DV-III+ viscometer. Measurements of phase transition temperatures, melting and freezing points were carried out on a Mettler-Toledo differential scanning calorimeter, model DSC822e, at a scan rate of 5 °C min<sup>-1</sup>, and the data were evaluated using the Mettler-Toledo STARE software version 7.01. FT-IR spectra were recorded on a Thermo Nicolet 5700 FTIR spectrophotometer. The water content was determined by Karl-Fisher analysis (Metrohm KF coulometer). The surface tension was measured on a surface/interface analytical device (Solon Tech. (Shanghai)) using the Du Noüy ring method. Contact angle data were obtained by a SEO Contact Angle Measuring Device (PHOENIX 300). X-Ray Photoelectron Spectroscopy (XPS) analyses were performed on a VG ESCA-LAB 210 instrument with an MgK $\alpha$  source (1253.6 eV) and calibrated *versus* the C 1s peak at 285.0 eV. A thin layer of  $\text{Fe}_2\text{O}_3$ /[EMIm][BF<sub>4</sub>] was deposited on a polycrystalline gold substrate, and was kept under moderate vacuum for at least 12 h before introduction into the analytical chamber of the XPS instrument. Spectrometer pass energies of 100 eV for the survey spectra and 30 eV for high resolution spectra were used for all elemental spectral regions. The pressure in the analyser chamber was 10<sup>-9</sup> Torr. X-Ray diffraction (XRD) was measured on a Siemens D/max-RB powder X-ray Diffractometer. Diffraction patterns were recorded with Cu K $\alpha$  radiation (30 mA, 40 kV) over a 2 $\theta$  range of 15° to 90° and a position-sensitive detector using a step size of 0.017°. Scanning electron microscopy (SEM) was carried out with a JSM-5600LV Vacuum Scanning Electron Microscope. Transmission electron microscopy (TEM) micrographs were taken on a Tecnai™ G<sup>2</sup>F30, FEI, USA. Room temperature magnetization isotherms were obtained using a vibrating sample magnetometer (VSM, LakeShore 7304).

### Preparation of ionic liquid marble

Liquid marbles were prepared by dropping IL droplets using a 10–100  $\mu\text{L}$  syringe onto a bed of PTFE powder (6–10  $\mu\text{m}$ ) layered in an agate mortar, and subsequently shaking the droplet gently so that the powder spontaneously covered the entire droplet surface. The excess particles are then shed by rolling the drop in a glass dish resulting in a liquid marble. Contact angles for IL droplets were obtained by a SEO Contact Angle Measuring Device (PHOENIX 300).

The directed movement of the liquid marbles was recorded using a digital charge-coupled device CCD camera.

### 3. Results and discussion

#### Synthesis and characterization of $\text{Fe}_2\text{O}_3@[\text{EMIm}][\text{BF}_4]$ and $\text{Fe}_2\text{O}_3$

$\text{Fe}_2\text{O}_3$  nanoparticles were obtained through facile, and energy-saving (100 mW) ultrasonic decomposition of  $\text{Fe}(\text{CO})_5$  in ILs in the absence of any other stabilizing surfactants and capping agents and solvents, which resulted in a stable composite  $\text{Fe}_2\text{O}_3$  nanoparticles/ILs system (denoted as  $\text{Fe}_2\text{O}_3@[\text{EMIm}][\text{BF}_4]$ ). Under ultrasonication, the mixture was first changed into yellow and then black solution, which indicated the formation of iron oxide nanoparticles. The decomposition of  $\text{Fe}(\text{CO})_5$  was monitored by the FTIR spectra. As shown in Fig. 1, different from the  $\nu_{\text{CO}}$  band of pure  $\text{Fe}(\text{CO})_5$  at 2034 ( $E'$  mode) and 2014 ( $A_2''$  mode)  $\text{cm}^{-1}$ ,<sup>33</sup> both modes of  $\text{Fe}(\text{CO})_5$  in  $[\text{EMIm}][\text{BF}_4]$  shifted to lower frequencies, at 1998 and 2015  $\text{cm}^{-1}$ , respectively, which is rather similar to the case of  $\text{Fe}(\text{CO})_5$  in a nonpolar solvent.<sup>33</sup> After ultrasonication for 1.5 h, the IR bands were disappeared, confirming the complete decomposition of  $\text{Fe}(\text{CO})_5$ . The concentration of  $\text{Fe}_2\text{O}_3$  in the resulted solution was 2% calculated by a weighting method, much less than the theoretic value of 2.8%, which was probably due to the evaporation of  $\text{Fe}(\text{CO})_5$  (bp 103 °C) caused by local heating under ultrasonic irradiation. The IR spectrum of  $\text{Fe}(\text{CO})_5 + [\text{EMIm}][\text{BF}_4]$  after ultrasonication for 1.5 h similar to the case of pure  $[\text{EMIm}][\text{BF}_4]$  further supported this. However, it should be noted that the low concentration of magnetic iron oxide nanoparticles did not limit the transport of the ionic liquid marble, as discussed below.

The physicochemical properties of the resulted  $\text{Fe}_2\text{O}_3@[\text{EMIm}][\text{BF}_4]$  were investigated and compared with that of  $[\text{EMIm}][\text{BF}_4]$ , as summarized in Table 1. It was found that introduction of  $\text{Fe}_2\text{O}_3$  nanoparticles preserves the attractive features of pure IL such as

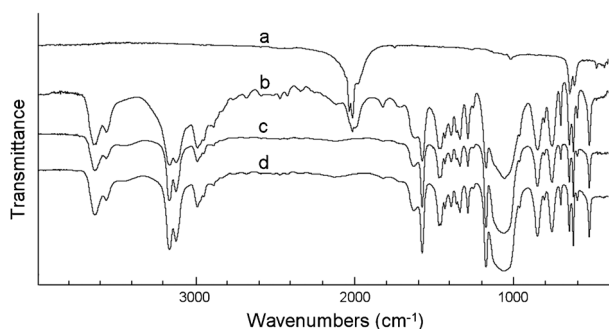


**Fig. 1** IR spectra of  $\text{Fe}_2\text{O}_3@[\text{EMIm}][\text{BF}_4]$ . (a)  $\text{Fe}(\text{CO})_5$ , (b)  $\text{Fe}(\text{CO})_5 + [\text{EMIm}][\text{BF}_4]$ , ultrasonication for 5 min, (c)  $\text{Fe}(\text{CO})_5 + [\text{EMIm}][\text{BF}_4]$ , ultrasonication for 1.5 h, (d)  $[\text{EMIm}][\text{BF}_4]$ .

**Table 1** Surface tension ( $\gamma$ ), density ( $\rho$ ), and viscosity ( $\eta$ ) of  $[\text{EMIm}][\text{BF}_4]$  and  $\text{Fe}_2\text{O}_3@[\text{EMIm}][\text{BF}_4]$

ILs	$\sigma/\text{mS cm}^{-1}$	$\gamma/\text{mN m}^{-1}$	$\rho/\text{g cm}^{-3}$	$\eta/\text{mPa m}^{-1}$
$[\text{EMIm}][\text{BF}_4]$	24.7	49	1.271	33
$\text{Fe}_2\text{O}_3@[\text{EMIm}][\text{BF}_4]$	22.3	51	1.282	40

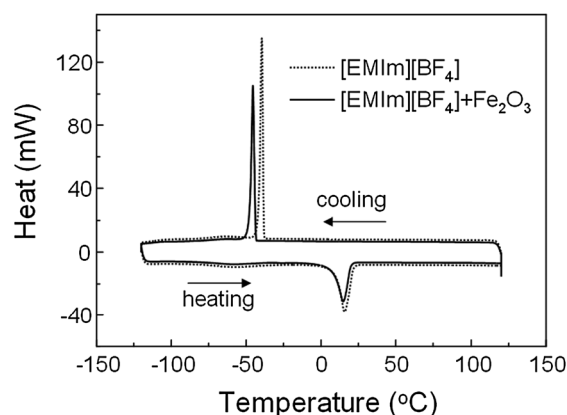


**Fig. 2** DSC curves of  $[\text{EMIm}][\text{BF}_4]$  and  $\text{Fe}_2\text{O}_3@[\text{EMIm}][\text{BF}_4]$ . The sample was first cooled and then heated at a rate of  $10\text{ °C min}^{-1}$ .

the high conductivity while slightly increasing the viscosity and density. The increase in surface tension was also observed. In order to address this issue, water contents of ILs before and after ultrasonic decomposition were measured, since the surface tension of ILs appear to be sensitive to the water content only beyond a given threshold value of water content (above 500 ppm).<sup>34</sup> However, below the threshold value the surface tension of ILs is not very sensitive to the presence of small amounts of water, since the residual water is probably tightly bound to the polar network and is not segregated from the surface, in particular for hydrophilic ILs.<sup>34</sup> The water content was found to increase from 536 ppm to 4636 ppm during the vigorous ultrasonication, which could be due to the open experimental set-up exposed to air and moisture. Thus the water absorption by hydrophilic  $[\text{EMIm}][\text{BF}_4]$  could be ascribed to increase in surface tension.

DSC curves of  $[\text{EMIm}][\text{BF}_4]$  and  $\text{Fe}_2\text{O}_3@[\text{EMIm}][\text{BF}_4]$  are shown in Fig. 2. As compared to the pure IL, the melting point of  $\text{Fe}_2\text{O}_3@[\text{EMIm}][\text{BF}_4]$  was kept constant at 15 °C, while the crystallizing temperature was depressed by *ca.* 6 °C due to the presence of  $\text{Fe}_2\text{O}_3$  nanoparticles. Actually, the decrease in crystallizing temperature was unclear at this stage. The presence of  $\text{Fe}_2\text{O}_3$  nanoparticles may influence the coulombic interaction and disturb the hydrogen bonding network in ILs, thus depressing the formation of the regular crystal and decreasing the crystallizing temperature.

The  $\text{Fe}_2\text{O}_3@[\text{EMIm}][\text{BF}_4]$  was directly subject to XPS analysis under ultra-high vacuum conditions. Fig. 3 shows the overview scan of a  $[\text{EMIm}][\text{BF}_4]$  film containing  $\text{Fe}_2\text{O}_3$ . From the survey spectrum in Fig. 3a, the expected elements B, C, N and F ascribed to  $[\text{EMIm}][\text{BF}_4]$  were all detected. In contrast, there is only weakly detectable signal of element Fe2p, as shown in Fig. 3b, in particular as compared to the case of XPS result of  $\text{Fe}_2\text{O}_3$  isolated from  $[\text{EMIm}][\text{BF}_4]$ . This could be due to the following reasons: (1) the low concentration of  $\text{Fe}_2\text{O}_3$ ; (2) the deposition of  $\text{Fe}_2\text{O}_3$  nanoparticles from the surface of ILs film during measurement; (3) encapsulation of  $\text{Fe}_2\text{O}_3$  by  $[\text{EMIm}][\text{BF}_4]$ . According to the XPS intensities of various elements, we deduced the atomic ratio of five elements as follows: B:C:F:Fe:N:O = 1:13.3:4.7:0.03:2.0:3.0 (the theoretical ratio of B:C:F:N is 1:6:4:2). The higher intensities of C and O than the theoretical values, as usually observed in the XPS result of ILs,<sup>35</sup> may

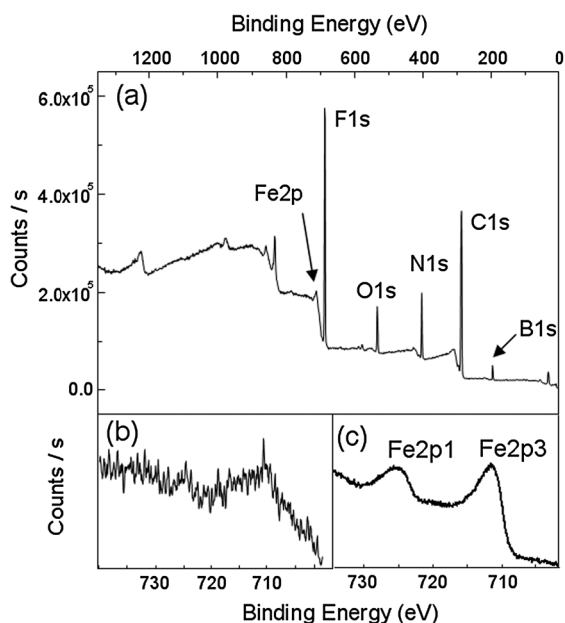


**Fig. 3** Survey XPS spectra of [EMIm][BF<sub>4</sub>] containing Fe<sub>2</sub>O<sub>3</sub> (a) and high-resolution spectra dealing with the Fe 2p photoemission from (b) and pure Fe<sub>2</sub>O<sub>3</sub> (c).

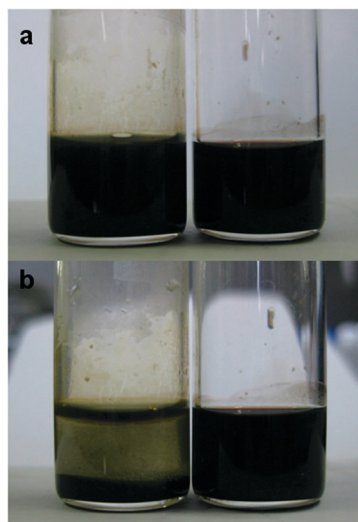


**Fig. 4** Stability of Fe<sub>2</sub>O<sub>3</sub> in a mixture of [EMIm][BF<sub>4</sub>] and water (left, 50 v/v% water) and in [EMIm][BF<sub>4</sub>] (right) in the presence of an applied magnetic field. The permanent magnet is placed below the flasks containing the MIL. (a) and (b) refer to pictures taken at  $t = 0$  and 10 min, respectively.

be caused by trace organic contaminations introduced during synthesis and measurement. The surface concentration of Fe<sub>2</sub>O<sub>3</sub> calculated by the atomic ratio was 1.5%, which is lower than the bulk concentration.

As shown in Fig. 4, the Fe<sub>2</sub>O<sub>3</sub>@[EMIm][BF<sub>4</sub>] is stable in the presence of a magnetic field, however, adding of water to the solution leads to aggregation and sedimentation of the Fe<sub>2</sub>O<sub>3</sub> nanoparticles in the applied magnetic field. Recent studies of colloidal stability without stabilizers in ILs focused on three different repulsive interactions between colloidal particles; electrostatic, steric, and solvation forces.<sup>36</sup> The electrostatic

charge stabilization appears to be insufficient owing to the high ionic strength of the ILs and the resulting surface-charge screening.<sup>36,37</sup> Alternatively, the steric and solvation forces effectively stabilize colloidal particles in ILs. As for the steric force, IL molecules (ions) that are strongly attached to colloidal surfaces may be bulky enough to separate each colloidal surface in certain cases. In this case, the nonpolar alkyl chains appeared to work as a protective group that prevents aggregation. For the IL-based solvation force,<sup>37</sup> the multilayered structure of ILs leads to the solvation force inducing longer-range repulsion as compared to the IL-based steric force. Smith *et al.* recently reported the long-term stability of charged silica particles in a protic IL, ethylammonium nitrate, where the solvation force was found to be responsible for this surprising stabilization.<sup>37</sup> They found that the suspensions become unstable in the presence of a small amount of water, and the destabilization was again evidenced by the decreased solvation force upon the addition of water. As for the case of Fe<sub>2</sub>O<sub>3</sub> nanoparticles in ILs investigated in this work, there is still destabilization when adding water, thus the Fe<sub>2</sub>O<sub>3</sub> nanoparticles can be regarded as stabilized by the solvation force in the ILs. The mechanism for coagulation of Fe<sub>2</sub>O<sub>3</sub> nanoparticles dispersed in [EMIm][BF<sub>4</sub>] with addition of water could be ascribed to the decreased solvation force upon the addition of water, similar to the case of charged silica particles in a protic IL.<sup>37</sup> The water-induced destabilization may be useful for separation of magnetic particles from the ionic liquid after transportation. Based on this method, the Fe<sub>2</sub>O<sub>3</sub> nanoparticles were isolated by addition of water, followed by centrifugation at 10 000 rpm for 10 min, and then washed three times with ethanol. The resulted Fe<sub>2</sub>O<sub>3</sub> nanoparticles were then investigated by TEM, XRD, XPS and susceptibility measurements.

The size of Fe<sub>2</sub>O<sub>3</sub> nanoparticles was measured using TEM, as shown in Fig. 5. It is found that the size distribution of the maghemite nanoparticles is from 2 to 6 nm. However, large agglomerates of Fe<sub>2</sub>O<sub>3</sub> nanoparticles are present, similar to the case of Fe nanoparticles obtained in [BMIm][BF<sub>4</sub>] in the absence of stabilizers,<sup>5</sup> which is mainly caused by their magnetic properties. Fig. 5 illustrates the XRD patterns obtained from Fe<sub>2</sub>O<sub>3</sub> nanoparticles. The sample exhibited peaks at around 30.2°, 35.7°, 43.6°, 53.7°, 57.3°, 62.9° corresponding to the (220), (311), (400), (422), (511), (440) reflections of  $\gamma$ -Fe<sub>2</sub>O<sub>3</sub>, which is in correspondence with those of No. 39–1346 in Powder Diffraction File (PDF) collected by the Joint Committee on Powder Diffraction Standards (JCPDS).<sup>38</sup>

The magnetization variation of the Fe<sub>2</sub>O<sub>3</sub> nanoparticles as a function of applied field at room temperature is shown in Fig. 6.

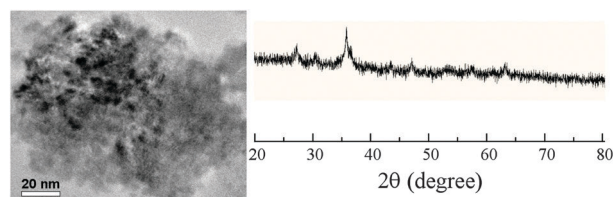


**Fig. 5** TEM image (left) and X-ray diffraction patterns (right) of iron oxide nanoparticles. Samples for TEM observations were prepared by placing a drop of an ethanolic solution containing the nanoparticles in a carbon coated copper grid.

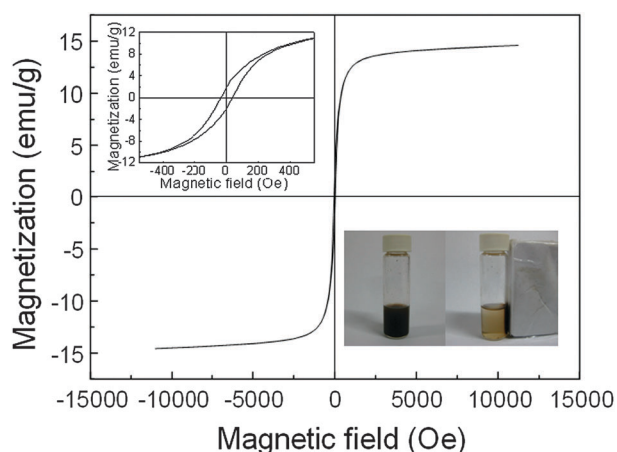


**Fig. 6** Magnetization curves of  $\text{Fe}_2\text{O}_3$  nanoparticles at room temperature. Inset (left) shows the expanded low field region of the hysteresis loop. Inset (right) shows the attraction of  $\text{Fe}_2\text{O}_3$  by a magnetic bar in ethanol.

The magnetization of the sample can be completely saturated at high fields of up to 1.1 T at room temperature with a saturation magnetization of  $M_s$  of  $14.5 \text{ emu g}^{-1}$ . Moreover, in comparison with superparamagnetic nanoparticles (hysteresis was absent with zero remanence and coercivity at room temperature), we find that this material has coercivity ( $H_c$ ) as shown in the expanded hysteresis loop between  $-550$  and  $+550 \text{ Oe}$ , which was evaluated to be  $35.6 \text{ Oe}$ , which indicated that the nanoparticles are of ferrimagnetic nature. The inset photograph indicates that the iron oxide nanoparticles in ethanol can be readily attracted and separated by an external magnetic field. In combination with the above result of XPS, XRD and magnetic properties, the iron oxide nanoparticles were assigned to  $\gamma\text{-Fe}_2\text{O}_3$ .

### Magnetic ionic liquid marble

As indicated by the SEM image (Fig. 7A and Fig. S1, ESI $\dagger$ ), the PTFE particles have irregular non-spherical shape with the median particle diameter (max.) of  $7.3 \mu\text{m}$ . Individual magnetic ionic liquid marble was prepared by rolling a droplet of  $\text{Fe}_2\text{O}_3/[\text{EMIm}][\text{BF}_4]$  over the PTFE powder. The PTFE powder immediately coated the droplet and rendered it both hydrophobic and non-wetting. However, a comparable experiment using polyvinylidene fluoride (PVDF) as superhydrophobic powder was unsuccessful due to the dissolution

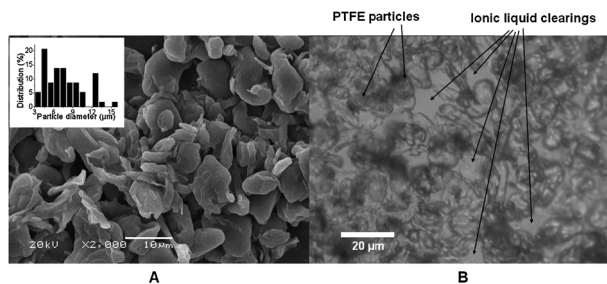


**Fig. 7** (A) SEM microscopy of PTFE particles (inset is the particle size distribution histogram). (B) Surface of an ionic liquid marble coated with PTFE particles, as seen with a microscope.

of PVDF in  $[\text{EMIm}][\text{BF}_4]$ . The ‘magnetic ionic liquid marbles’ remained intact and in a perfectly non-wetting state after transfer onto a solid surface (PTFE, glass and paper) or liquid surface (water), where they become highly mobile. On the water surface, the adsorbed PTFE powder at the air–water surface of the ‘ionic liquid marbles’ prevents diffusion of ILs between the ‘marble’ interior and the bulk liquid water. In order to study the packing situation of the PTFE particles adsorbed onto the ionic liquid interface, the top face of the ionic liquid marble was investigated by optical microscopy. Although it seems that the PTFE particles are close-packed from the images with low resolution (Fig. S2, ESI $\dagger$ ), the image with high resolution (Fig. 7B) demonstrates that the PTFE particles are separated by ionic liquid clearings (empty areas, as indicated by the arrows), which is consistent with the results obtained in water marbles.<sup>15,17,39</sup> Thus it could be recognized that on the microscopic scale the PTFE particles do not adsorb onto the interface in a close-packed situation.

The shape of the liquid droplet was rationalized according to the relationship between the quasi-spherical radius ( $R_0 = (3V/4\pi)^{1/3}$ ) and the capillary length ( $k^{-1} = (\gamma/\rho g)^{1/2}$ ) of the liquid droplet. For  $R_0 \ll k^{-1}$ , the liquid droplet kept the quasi-spherical shape, while for  $R_0 \gg k^{-1}$ , the larger marbles were deformed by gravity and become puddle shaped, where  $V$ ,  $\gamma$ ,  $\rho$  and  $g$  are the volume of the liquid droplet, surface tension, density of liquid and the acceleration due to gravity, respectively.

Using the data in Table 1,  $k^{-1}$  of the  $\text{Fe}_2\text{O}_3/[\text{EMIm}][\text{BF}_4]$  droplets is calculated to be  $2.0 \text{ mm}$ . This result suggests that a small magnetic ionic liquid marble should have a near-spherical shape and large marble adopt a puddle shape, which was confirmed by the experimental results shown in Fig. 8. A  $10 \mu\text{L}$   $\text{Fe}_2\text{O}_3/[\text{EMIm}][\text{BF}_4]$  marble ( $R_0 = 1.33 \text{ mm}$ ) deposited on the PTFE surface maintains its sphericity with contact angle as high as  $154^\circ$ , while a  $200 \mu\text{L}$  marble ( $R_0 = 3.6 \text{ mm}$ ) has a puddle shape.

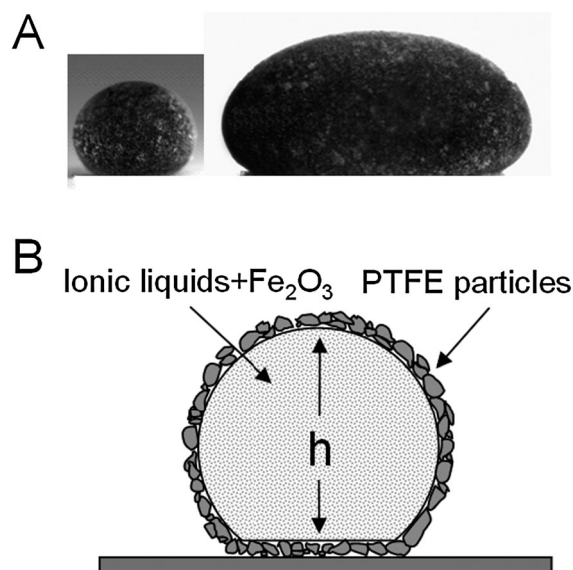


**Fig. 8** (A) Magnetic ionic liquid marble deposited on the flat polyethylene substrate (left:  $10 \mu\text{L}$ ,  $h = 2.35 \text{ mm}$ ; right:  $200 \mu\text{L}$ ,  $h = 3.91 \text{ mm}$ ). (B) Scheme of the magnetic ionic liquid marble.

According to established procedures, the effective surface tension ( $\gamma$ ) of the magnetic ionic liquid marble could be determined by the maximal height ( $H$ ) of a puddle shape, using eqn (1):<sup>15,40–42</sup>

$$\gamma = \frac{\rho g H^2}{4} \quad (1)$$

The limiting value of the puddle height provides an estimate of the surface tension of  $48 \pm 2 \text{ mN m}^{-1}$ , which is rather close to the theoretical value of  $50 \text{ mN m}^{-1}$  (wherein  $H$  tends asymptotically to twice the capillary length<sup>11,43</sup>) and surface tension of  $\text{Fe}_2\text{O}_3@[\text{EMIm}][\text{BF}_4]$ . Moreover, because of the lack of effective surface tension of ionic liquid marble, and the report that  $\gamma$  of the water marble depends strongly on the kind of powder coating the marble and also the measuring method,<sup>40</sup> the  $\gamma$  obtained here can only be compared with that water marble coated with the same powder and method. The effective surface tension of the magnetic ionic liquid marble is obviously less than that of water marble coated with PTFE powder ( $60 \text{ mN m}^{-1}$ ),<sup>40</sup> which could be due to its lower surface tension as compared to water.

Although water marble coated with the same PTFE powder possesses contact angle ( $164^\circ$ ) higher than that of magnetic ionic liquid marble, the lifetime of water marble was shorter than 20 min at room temperature. As shown in Fig. 9, slow evaporation of the water droplet led to the appearance of first wrinkles on the droplet surface and eventual collapse. In contrast, the ionic liquid marble, which was said to remain floating on a water surface for a week,<sup>28</sup> showed nearly no obvious deformation. However, dropping a droplet of organic liquid with low surface tension such as dodecane into water destroyed the magnetic ionic liquid marble immediately. The reason for the marbles destruction is quite clear. Dodecane formed low surface tension oil film spread on a water surface. This film contacting PTFE particles enwrapping the marble possesses a low surface tension. Thus, it turned out to be energetically favorable for PTFE particles to disconnect from a high energy water surface of a marble and to adhere to oil contaminants.<sup>20</sup> This property can be used to destroy an ionic liquid marble after its transportation.

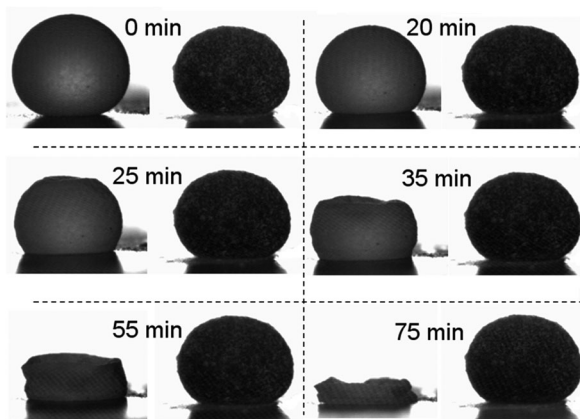


**Fig. 9** Digital photographs of  $10 \mu\text{L}$  water marble (left) and magnetic ionic liquid marble (right) placed on a PTFE substrate at room temperature.

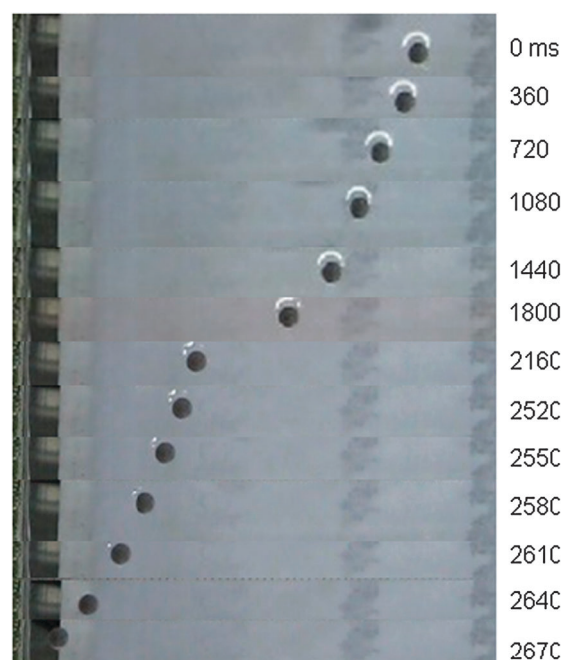


**Fig. 10** Still frames from a video showing the movement of a  $10 \mu\text{L}$  magnetic ionic liquid marble on a water surface. The liquid marble moves horizontally from left to right to impact a glass wall by the action of a permanent magnet.

Fig. 10 shows the magnetically actuated ionic liquid marble moving on a water surface (video 1 in ESI†). The magnet bar was placed on the left side and moved slowly toward the liquid marble until the marble started to move. The critical magnetic field actuating the droplet motion was  $2.2 \text{ mT}$ . The distance the liquid marble moved was  $65 \text{ mm}$ . It is noted that the minimal force needed to actuate the liquid marble should be determined by the maximum static friction between the marble and the water surface. Herein, the magnetic force acting on the liquid marble is proportional to the intensity of external magnetic field ( $2.2 \text{ mT}$ ) and the mass of magnetic powder on the droplet ( $0.256 \text{ mg}$ ). Under the action of the static magnetic field, the movement of the droplet sped up to a velocity of  $1.47 \text{ cm s}^{-1}$  before it impacted the glass wall (the velocity was obtained as the first-order derivative of the displacement ( $S$ )–time ( $t$ ) equation). In this case, no detachment of  $\text{Fe}_2\text{O}_3$  particles from the liquid marble was observed. These results indicate that the as-prepared liquid marbles are robust enough for manipulation of liquid transport in microfluidic devices. However, the magnetic ionic liquid marble cannot be transported on the solid substrate such as PTFE and paper, which is mainly due to the weak magnetic intensity of the overall composite system (the normalized  $M_s$  is  $0.29 \text{ emu g}^{-1}$  when considering  $\gamma\text{-Fe}_2\text{O}_3$  dispersed in IL) and the increased frictional force as compared to the liquid surface. The transportation on a solid substrate will be achieved by increasing the concentration of  $\text{Fe}_2\text{O}_3$  in IL or by using a pure magnetic IL.<sup>44,45</sup> Our preliminary result confirmed that  $[\text{BMIm}][\text{FeCl}_4]$  formed magnetic ionic liquid marble upon coating with PTFE powder, which can be easily transported on a glass substrate with a constant rate of up to  $2.5 \text{ cm s}^{-1}$  under magnetic actuation (video 2 in ESI†).

## 4. Conclusions

In summary, facile synthesis of iron oxide nanoparticles in ILs was obtained through ultrasonic decomposition of iron carbonyl precursors in ILs without any stabilizing or capping agents. The formation of Fe<sub>2</sub>O<sub>3</sub> nanoparticles in IL made the suspension system magnetic while the suspension preserves the features of IL such as high conductivity and surface tension. The resulted Fe<sub>2</sub>O<sub>3</sub>@[EMIm][BF<sub>4</sub>] system can be further directly used as magnetic ionic liquid marble, which can be transported readily with magnetic actuation. Our work demonstrated a facile method for the synthesis of iron oxide nanoparticles in ILs and preparation of magnetic ionic liquid marbles. This approach can be expanded to other general ILs and also magnetic ILs themselves, which will open the way to easy low-volume manipulation of ILs on a flat surface without prepatterned surfaces or electrical contacts.

## Acknowledgements

This work was supported by the financial support of National Natural Science Foundation of China (No. 21103208 and 21173240). The authors would like to thank Prof. Bin Hu and Mr Xumao Xiong for kind supply of iron pentacarbonyl, and Ms Ling Gao, Ms Li He, Mr Qixiu Zhu and Mr Jiazheng Zhao for XPS, XRD, NMR and SEM characterization.

## Notes and references

- M. J. Earle and K. R. Seddon, *Pure Appl. Chem.*, 2000, **72**, 1391–1398.
- J. H. Davis and P. A. Fox, *Chem. Commun.*, 2003, 1209–1212.
- Ionic liquids in synthesis*, ed. P. Wasserscheid and T. Welton, Wiley-VCH, Weinheim, Germany, 2003.
- L. Lartigue, R. Pflieger, S. I. Nikitenko, Y. Guari, L. Stievano, M. T. Sougrati and J. Larionova, *Phys. Chem. Chem. Phys.*, 2011, **13**, 2111–2113.
- J. Kramer, E. Redel, R. Thomann and C. Janiak, *Organometallics*, 2008, **27**, 1976–1978.
- C. M. Lee, H. J. Jeong, S. T. Lim, M. H. Sohn and D. W. Kim, *ACS Appl. Mater. Interfaces*, 2010, **2**, 756–759.
- J. B. Lian, X. C. Duan, J. M. Ma, P. Peng, T. I. Kim and W. J. Zheng, *ACS Nano*, 2009, **3**, 3749–3761.
- E. Redel, R. Thomann and C. Janiak, *Chem. Commun.*, 2008, 1789–1791.
- Y. Wang, S. Maksimuk, R. Shen and H. Yang, *Green Chem.*, 2007, **9**, 1051–1056.
- H. Hu, H. Yang, P. Huang, D. Cui, Y. Peng, J. Zhang, F. Lu, J. Lian and D. Shi, *Chem. Commun.*, 2010, **46**, 3866–3868.
- P. Aussillous and D. Quere, *Nature*, 2001, **411**, 924–927.
- A. B. Subramaniam, M. Abkarian and H. A. Stone, *Nat. Mater.*, 2005, **4**, 553–556.
- A. B. Subramaniam, C. Mejean, M. Abkarian and H. A. Stone, *Langmuir*, 2006, **22**, 5986–5990.
- E. Bormashenko, R. Pogreb, Y. Bormashenko, A. Musin and T. Stein, *Langmuir*, 2008, **24**, 12119–12122.
- P. Aussillous and D. Quere, *Proc. R. Soc. A*, 2006, **462**, 973–999.
- M. Dandan and H. Y. Erbil, *Langmuir*, 2009, **25**, 8362–8367.
- E. Bormashenko, R. Pogreb, G. Whyman, A. Musin, Y. Bormashenko and Z. Barkay, *Langmuir*, 2009, **25**, 1893–1896.
- D. Dupin, S. P. Armes and S. Fujii, *J. Am. Chem. Soc.*, 2009, **131**, 5386–5387.
- J. R. Dorvee, A. M. Derfus, S. N. Bhatia and M. J. Sailor, *Nat. Mater.*, 2004, **3**, 896–899.
- E. Bormashenko and A. Musin, *Appl. Surf. Sci.*, 2009, **255**, 6429–6431.
- Y. Zhao, J. Fang, H. X. Wang, X. G. Wang and T. Lin, *Adv. Mater.*, 2010, **22**, 707–710.
- Y. H. Xue, H. X. Wang, Y. Zhao, L. M. Dai, L. F. Feng, X. G. Wang and T. Lin, *Adv. Mater.*, 2010, **22**, 4814–4818.
- J. F. Tian, T. Arbatan, X. Li and W. Shen, *Chem. Commun.*, 2010, **46**, 4734–4736.
- J. F. Tian, T. Arbatan, X. Li and W. Shen, *Chem. Eng. J.*, 2010, **165**, 347–353.
- E. Bormashenko, R. Balter and D. Aurbach, *Appl. Phys. Lett.*, 2010, **97**, 091908.
- S. Fujii, S. Kameyama, S. P. Armes, D. Dupin, M. Suzuki and Y. Nakamura, *Soft Matter*, 2010, **6**, 635–640.
- E. Bormashenko, R. Pogreb and A. Musin, *J. Colloid Interface Sci.*, 2012, **366**, 196–199.
- L. C. Gao and T. J. McCarthy, *Langmuir*, 2007, **23**, 10445–10447.
- E. Altin, J. Gradl and W. Peukert, *Chem. Eng. Technol.*, 2006, **29**, 1347–1354.
- C. Guerrero-Sanchez, T. Lara-Ceniceros, E. Jimenez-Regalado, M. Raza and U. S. Schubert, *Adv. Mater.*, 2007, **19**, 1740–1747.
- N. Jain, X. Zhang, B. S. Hawkett and G. G. Warr, *ACS Appl. Mater. Interfaces*, 2011, **3**, 662–667.
- F. C. C. Oliveira, L. M. Rossi, R. F. Jardim and J. C. Rubim, *J. Phys. Chem. C*, 2011, **113**, 8566–8572.
- K. M. Rao, G. Spoto, E. Guglielminotti and A. Zecchina, *Inorg. Chem.*, 1989, **28**, 243–247.
- M. Tariq, M. G. Freire, B. Saramago, J. A. P. Coutinho, J. N. C. Lopes and L. P. N. Rebelo, *Chem. Soc. Rev.*, 2012, **41**, 829–868.
- Q. H. Zhang, S. M. Liu, Z. P. Li, J. Li, Z. J. Chen, R. F. Wang, L. J. Lu and Y. Q. Deng, *Chem.–Eur. J.*, 2009, **15**, 765–778.
- K. Ueno and M. Watanabe, *Langmuir*, 2011, **27**, 9105–9115.
- J. A. Smith, O. Werzer, G. B. Webber, G. G. Warr and R. Atkin, *J. Phys. Chem. Lett.*, 2010, **1**, 64–68.
- Y. P. He, Y. M. Miao, C. R. Li, S. Q. Wang, L. Cao, S. S. Xie, G. Z. Yang, B. S. Zou and C. Burda, *Phys. Rev. B: Condens. Matter*, 2005, **71**, 125411.
- T. H. Nguyen, K. Hapgood and W. Shena, *Chem. Eng. J.*, 2010, **162**, 396–405.
- E. Bormashenko, R. Pogreb, G. Whyman and A. Musin, *Colloids Surf., A*, 2009, **351**, 78–82.
- E. Bormashenko, *Curr. Opin. Colloid Interface Sci.*, 2011, **16**, 266–271.
- S. Fujii, M. Suzuki, S. P. Armes, D. Dupin, S. Hamasaki, K. Aono and Y. Nakamura, *Langmuir*, 2011, **27**, 8067–8074.
- M. I. Newton, D. L. Herbertson, S. J. Elliott, N. J. Shirtcliffe and G. McHale, *J. Phys. D: Appl. Phys.*, 2007, **40**, 20–24.
- S. Hayashi and H. O. Hamaguchi, *Chem. Lett.*, 2004, 1590–1591.
- T. Peppel, M. Kockerling, M. Geppert-Rybczynska, R. V. Ralys, J. K. Lehmann, S. P. Verevkin and A. Heintz, *Angew. Chem., Int. Ed.*, 2010, **49**, 7116–7119.